Reactivity of Calcite/Water-Interfaces (RECAWA): Molecular level process understanding for technical applications

Stelling J. (1), Neumann T.* (1), Kramar U. (1), Schäfer T. (2), Heberling F. (2), Winkler B. (3), Vinograd V. (3), Arbeck D. (3), Müller H.S. (4), Haist M. (4), Glowacky J. (4), Vucak M. (5), Fischer U. (6), Pust C. (6), Huber J. (7), Bosbach D. (8)

(1) Karlsruhe Institute of Technology (KIT), Institute of Mineralogy and Geochemistry (IMG), e-mail: stelling@kit.edu, neumann@kit.edu, utz.kramar@kit.edu

(2) Karlsruhe Institute of Technology (KIT), Institute for Nuclear Waste Disposal (INE), e-mail: thorsten.schaefer@kit.edu, frank.heberling@ine.fzk.de

(3) Goethe Universität Frankfurt (UF), Institut für Geowissenschaften (IfG), e-mail: b.winkler@kristall.uni-frankfurt.de, v.vinograd@kristall.uni-frankfurt.de, Arbeck@kristall.uni-frankfurt.de

(4) Karlsruhe Institute of Technology (KIT), Institute of Reinforced Concrete Structures and Building Materials (IfMB), e-mail: hsm@ifmb.uni-karlsruhe.de, haist@kit.edu, jens.glowacky@ifmb.uka.de

(5) Schaefer Kalk GmbH & Co. KG, e-mail: marijan.vucak@schaeferkalk.de

(6) Rheinkalk Akdolit GmbH & Co. KG, e-mail: uwe.fischer@rheinkalk.de, christopher.pust@rheinkalk.de

(7) Lafarge Zement Wössingen GmbH, e-mail: juergen.huber@lafarge-zement.lafarge.com

(8) Forschungszentrum Jülich GmbH, Institute of Energy Research (IEF), e-mail: d.bosbach@fz-juelich.de

*Coordinator of the project

Abstract

RECAWA intends to develop a fundamental understanding of the reactivity and dynamics of calcite surfaces during crystal growth in aquatic systems. Therefore, the calcite-water surface has been characterised at different hydrochemical conditions and surface diffraction measurements have been applied to probe if changes in zeta potential are accompanied by changes in the calcite-water interface structure. The interaction of calcite with Selenium is investigated in a mixed flow reactor (MFR) study which is accompanied by GI-EXAFS analyses to characterize the Se adsorption species.

The interaction of calcite surfaces with phosphate and phosphonates is the focus of two sub-projects. The sorption/precipitation mechanisms of PO_4^{3-} and HPO_3^{2+}, respectively, on different calcite powders (precipitated calcium carbonates and limestone powders) are investigated to determine sorption isotherms and phase transformations on the applied surfaces which is of great interest with regard to phosphate recycling and/or water treatment. Analytical work includes SEM, XRD and XAFS spectroscopy for a detailed characterisation of the calcite powders in different sections of the isotherms.

Experimental investigations on the interaction of limestone powder and two superplasticizers have been conducted with regard to concreting. These experiments were done at alkaline conditions and lead to massive reactions and changes in the zeta potential of the solutions and limestone powder when superplasticizers added.

Additional results of quantum-mechanical calculations and force-field modelling demonstrated that the Double Defect Method is able to quantitatively predict mixing properties of various iso-structural binary and ternary carbonate solid solutions. In particular, low equili-

brium retention levels of SO_4^{2-} and SeO_4^{2-} in carbonates imply that the reasonably large concentrations SO_4^{2-} and SeO_4^{2-} in carbonates reported in previous studies should be attributed to non-equilibrium entrapment effects.
Data obtained from atomistic modelling complement our data determined using lab methods. Further experimental and analytical, work including in-situ AFM studies using Iceland spar single crystals, is in progress and will help to interconnect the present results of the sub-projects.

1. Introduction

Carbonates are of high economic interest and represent an important resource for the chemical and pharmaceutical industry, glass and paper industry, construction material industry, for the production of fertilizers and for the quality of drinking water. Due to the abundance of carbonate rocks in the earth crust, carbonates are considered as a mineral mass product.
As the thermodynamically most stable and most abundant carbonate phase, calcite plays a prominent role for numerous natural processes in our environment. Calcite affects in various ways the global circulation of matter, regulates the pH and controls the chemical composition of natural aquatic systems, and has the ability to fix or structurally incorporate biologically active and, depending on the concentration, hazardous elements such as phosphorus, calcium, magnesium, iron, arsenic, selenium and other trace elements. Adsorption reactions are usually rather fast compared to co-precipitation reactions. In particular with respect to kinetic aspects of trace element sorption, the molecular level reactions at the mineral/water interface need to be understood in various fields of application to improve the effectiveness of industrial calcite mass products such as PCCs or filter material for water treatment. Atomistic models allow studying sorption of complexes and molecules at the mineral-water interface and the formation of solid solutions. These aspects of the interaction of calcite surfaces with dissolved reactants require different simulation approaches. Sorption processes are modelled using Molecular Dynamics, while solid solution formation is treated with statistical thermodynamic tools which combine quantum mechanical calculations and Monte Carlo simulations.
To achieve the goals of the joint research project, experimental and analytical work is divided in sub-projects which concentrate on different aspects of calcite surfaces.

2. The calcite-water surface and its interaction with Selenium

2.1. Structure and speciation of the calcite-water interface

To characterize the calcite surface potential as a function of the composition of the aqueous contact solution we measure calcite zeta potentials using two methods. (i) Electrokinetic measurements are performed in a Brookhaven Instruments zeta potential analyzer using phase analyses light scattering (PALS). For PALS measurements we use equilibrium solutions at three different CO_2 partial pressures, at atmospheric pressure. Suspensions are pre-equilibrated until the theoretically expected pH is reached. In equilibrium with pure CO_2 pH range is 5.8 to 6.8, in equilibrium with air (360 ppm CO_2) pH range is 7.5 to 9.6, and in equilibrium with N_2 (6 ppm CO_2) pH range is 8.4 to 10.3. We observe an increase in the iso-electric point (IEP) with decreasing CO_2 partial pressure. (ii) Streaming potential measurements are performed on an Anton Paar SurPASS electrokinetic analyzer. Streaming potential is measured as a function of pH performing pH titrations in a pH range from 5.5 to 11. As at these conditions solutions are undersaturated with respect to calcite, the calcite must be dissolving during the measurements. Solution analysis proofs, however, that this does not have a significant influence on the solution composition during the experiments. Hardly any pH dependence is observed in streaming potential measurements. Zeta potential increases with increasing Ca^{2+} concentration and decreases with increasing CO_3^{2-} concentration.

Table 2.1: Composition and chemical conditions in the contact solutions used for the surface diffraction study.

Dataset	1	2	3	4	5
solution state (eq. = equilibrium)	eq.: water - air - calcite	eq.: water - air - calcite	eq.: water - air - calcite	non- eq.	non- eq.
NaCl (mol/L)	-	0.097	0.03	0.01	0.01
additions (mol/L)	NaOH: 0.002	NaOH: 0.003	HCl 0.07	NaOH: 0.001	NaOH: 0.0005
				$CaCl_2$: 0.01	Na_2CO_3: 0.01
$p(CO_2)$ (ppm)	360	360	360	-	-
zetapotential (mV)	~ 0	~ 0	~ 9	~ 8	~ -25
pH	8.6±0.1	8.6±0.1	7.5±0.1	10.9±0.1	11.1±0.1

Surface diffraction measurements are applied to probe if changes in zeta potential are accompanied by changes in the calcite-water interface structure. We perform in-situ surface diffraction measurements at the GSECARS undulator beamline at sector 13 of the Advanced Photon Source. Five crystal truncation rod datasets are recorded at the solution conditions listed in Table 2.1.

Main results of the interface structure analyses are:

- The part of the calcite(104)–water interface structure, to which surface diffraction measurements are mainly sensitive, does not change significantly, even for the investigated extreme differences in the composition of the contact solutions.
- No indication for calcium or carbonate inner–sphere complexes on the flat calcite(104)–face is observed.
- Two well ordered layers of water are identified at 2.35±0.10 Å and 3.24±0.12 Å above the calcite surface. Water molecules of the first layer are located above the surface calcium ions and those of the second layer are located above the surface carbonate ions.
- In contact with solution mainly surface carbonate ions relax slightly from their bulk position and tilt towards the surface by about 4°.
- A gradual increase in Debye–Waller factors from the bulk crystal to the solution is observed.
- Elevated Debye–Waller factors of water molecules in the second water layer in datasets 3 and 4 (high Ca^{2+} concentration in solution), as well as the drop in diffuse electron density at about 4.2 Å above the surface in dataset 5 (no Ca^{2+} in solution), might be indicative for calcium outer–sphere complexes.

A Basic Stern Surface complexation model is developed that, in accordance with the interface structure analyses, considers only outer-sphere adsorption of ions other than protons and hydroxide. The observed zeta potentials are well reproduced by the model. A major advantage compared to previous models (*van Cappellen et al., 1993; Pokrovsky et al., 2000; Wolthers et al., 2008*) is that a physically reasonable value for the Helmholtz-Capacitance (0.45 F/m^2) is obtained. Together with the Stern layer thickness, estimated from the surface diffraction results (~3.5 Å), this value can be used to estimate the relative permittivity of the interface water, to be about 18.

2.2. Selenite ($Se(IV)O_3^{2-}$) and Selenate ($Se(VI)O_4^{2-}$) interaction with calcite

The MFR study on selenite / selenate coprecipitation is ongoing. MFR experiments at pH 7.4 show that the pH has an influence on the incorporation. As expected anion adsorption and subsequent incorporation is increased at lower pH. Partition coefficients at pH 7.4 are ~10^{-3} for selenate and ~10^{-2} for selenite, which still shows that selenium incorporation into calcite is unfavorable, but the values are relatively large compared to the extremely low values measured at pH 10.3, which were below the detection limit of the method.
Comparison of the macroscopic calcite growth

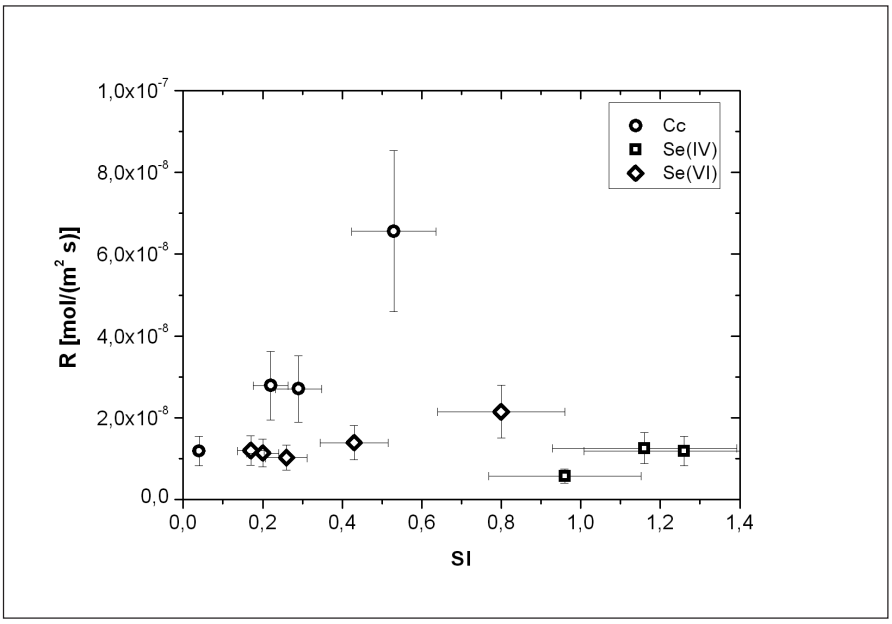

Figure 2.1: Macroscopic calcite growth rates obtained in MFR experiments on pure calcite (Cc, circles), in presence of selenite (Se(IV), squares), and selenate (Se(VI), diamonds).

rate obtained in MFR experiments in presence and absence of selenite / selenate (Fig. 2.1) shows the retarding effect, these anions have on calcite growth.

Selenium K-edge EXAFS is used to characterize the adsorption species of selenate at the calcite water interface. Adsorption samples are prepared in batch type adsorption experiments in pre-equilibrated calcite suspensions at pH 8.3 and 7.5 using calcite powder (Merck calcium carbonate suprapur) or freshly cleaved Iceland spar single crystal platelets as substrate. Initial SeO_4^{2-} concentration is 2×10^{-3} mol/L. EXAFS spectra measured on powder adsorption samples (black circles in Fig. 2.2) do, despite the lower signal to noise ratio, not deviate significantly from a reference EXAFS spectrum measured on a 0.1 mol/L $NaSeO_4$ solution (thick black line in Fig. 2.2). Therefore these spectra are considered inappropriate to characterize the adsorption species.
Only spectra measured on single crystal samples using grazing incidence to achieve surface sensitivity, show an additional contribution to the EXAFS most visible around k = 10.7 $Å^{-1}$ (dashed line in Fig. 2.2) that results in oscillations in the Fourier transform spectra between R = 2.7 Å and R = 3.7 Å. These are likely contributions to the adsorption species spectrum originating from the calcite surface. Detailed EXAFS data analysis is still in progress.

3. Fixation and phase transformation of phosphate at calcite surfaces

It is well known that phosphate is crucial for increased primary production, but its availability as a non-renewable resource is decreasing dramatically (*Gilbert, 2009; Driver et al., 1999*). On the other hand, severe environmental problems result through the discharge of nutrient rich waters from urban, agricultural and industrial sources. This leads to the eutrophication of water bodies and the enrichment of phosphate in sewage and wastewaters (*Smith, 2003*). Therefore, the immobilization of phosphate dissolved in eutrophic water bodies and wastewaters is a promising approach to solve this problem and to recycle phosphate.
In the past, calcite was used for the remediation of eutrophied water to immobilise dissolved phosphate (*Babin et al., 1994; Prepas et al, 1997; Hart et al., 2003*). Laboratory tests demonstrate the success of calcite application and show that a calcite barrier can reduce the

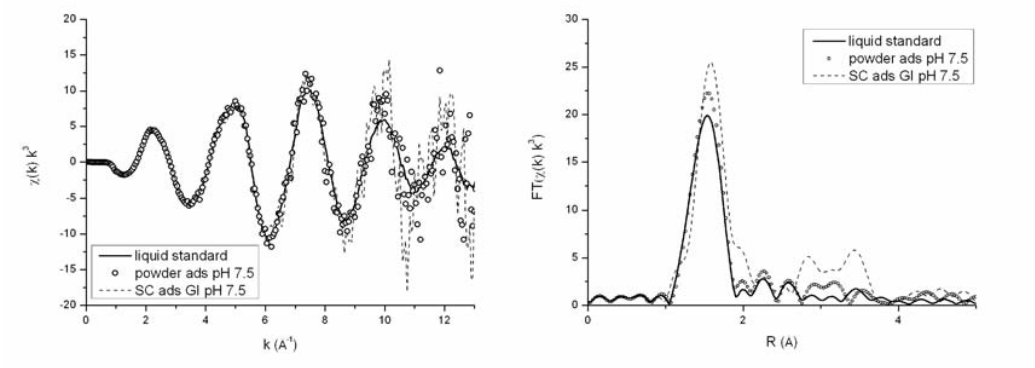

Figure 2.2: k3 weighted EXAFS (left) and Fourier Transform (right) spectra measured on: a liquid SeO_4^{2-} reference (thick black line), powder adsorption sample at pH 7.5 (circles), and single crystal adsorption sample measured at grazing incidence at pH 7.5 (dashed line).

phosphate flux from nutrient-rich sediments to the water. The mechanisms of phosphate fixation at the calcite surface are decisive for the efficiency and sustainability (*Babin et al., 1994; Berg et al., 2004*), but poorly understood at the atomic scale to date. Calcite has its point of zero charge between pH 8.0 and 9.5 (*Somasundaran & Agar, 1967*), while many other minerals have negative surfaces already at pH < 7. Hence, calcite exhibits a positive surface charge and can be used for anion adsorption.

A detailed explanation of the processes of phosphate fixation and phase transformation on calcite surfaces under varying hydrochemical conditions is investigated. The scientific and technical objectives cover:

i. the clarification of the mechanisms of phosphate fixation and phase transformations on calcite surfaces
ii. the characterisation of the hydrochemical conditions and crystallographic parameters for optimised and effective fixation of dissolved phosphate on calcite surfaces
iii. the identification and development of calcite products for the technical application

3.1. Experimental and analytical methods

The uptake of phosphate (PO_4^{3-}) by calcite from saturated calcite solutions has been examined using three types of calcite powders, (i) a powdered powder Devonian limestone (Sancy, FR) with a specific surface area of 1.76 m^2/g (SSA, estimated by N2-BET, sample A), (ii) precipitated $CaCO_3$ (*Merck p.a., 102066, 0.2* m^2/g; sample M), and (iii) a precipitated $CaCO_3$ delivered by Rheinkalk Akdolit (PCC, sample B, 37.45 m^2/g). Different amounts of calcite powder (0-50 g/L) were added to saturated calcite solutions (SI_{CaCO3} = 0.6 - 1.2, Ca^{2+} = 1.8 - 2.8 mmol/L, TA(HCO_3^-) = 4.0 - 8.0 mmol/L), produced from Merck p.a. chemicals ($CaCl_2$, $NaHCO_3$) and double-distilled H_2O (18.2 MΩ·cm) as described by Lin & Singer (2005). Phosphate was added in concentrations of 3 to 1000 µmol/L as H_3PO_4 or $Na_3PO_4{\times}6H_2O$. pH of the solutions was adjusted to 8.0 using HCl or NaOH. PO_4^{3-} concentrations of the calcite solutions are comparable to conditions of pore water and hypolimnion of eutrophic water bodies (*Belzile et al., 1996*). The batch solutions and the powders were shaken for 24 h (Fig. 3.1).

Afterwards the solutions and powders were separated by vacuum filtration. Residual concentrations of Ca^{2+} and PO_4^{3-} were analysed by AAS, ICP-OES and UV-VIS spectrophotometry, respectively. Total alkalinity (HCO_3^-) was chekked using an Aquamerck quick test (Merck 11109) and pH values were determined using a WTW SenTix 81 electrode attached to a WTW pH330 pH-meter. Changes in the morphology of the calcite sample powders were checked with REM. P concentrations and speciation of the powders were analysed by EDXRF and XANES spectroscopy, respectively.

3.2. Results

pH values remained stable at 8.10±0.15 during the experimental run. (Over)saturated calcite

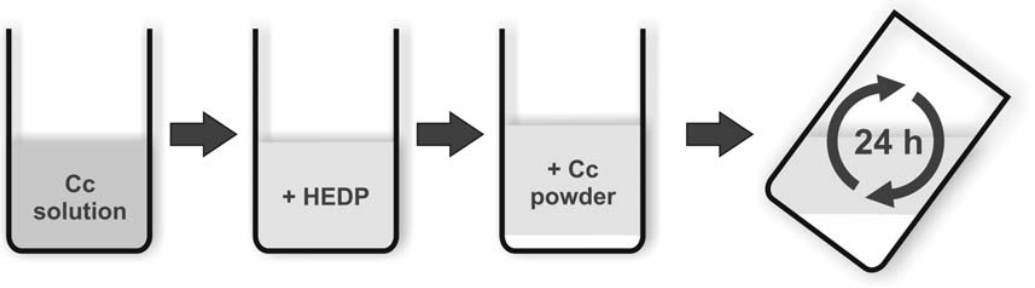

Figure 3.1: Scheme of a batch sorption experiments.

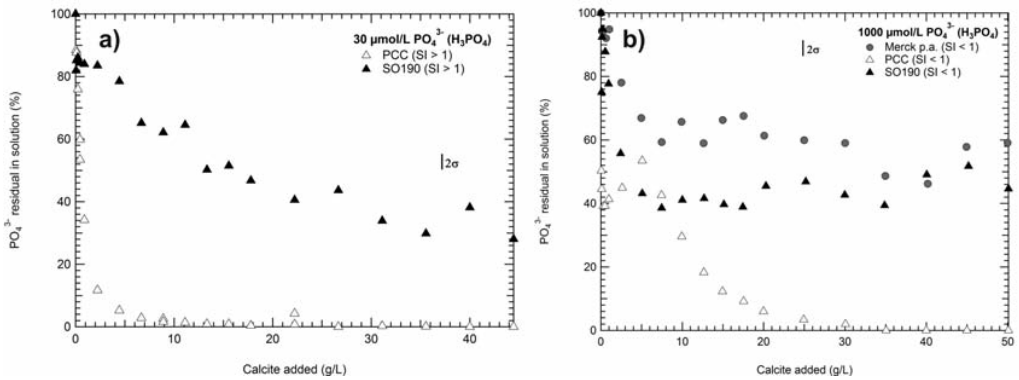

Figure 3.2: Normalized post-experimental PO_4^{3-} concentrations of experimental series starting with a) 30 µmol/L and 1000 µmol/L.

solutions show decreasing trends for Ca^{2+} and HCO_3^- and P concentrations in dependence of the SSA, respectively. Overall removal of phosphate from the batch solution ranges from 2 % to 100 %, dependent on the applied calcite powders. In contrast to experimental series of sample A and M, phosphate was eliminated from the batch solution of sample B series completely at all starting concentrations of 3 to 1000 µmol/L PO_4^{3-}. The addition of small amounts of calcite B (~10 g/L) results in a phosphate elimination of min. ~70 %, whereas calcite A and M result in a decrease of max. ~70 %. Adding high amounts of calcite powder to the batch solution (≥25 g/L) results in a complete phosphate elimination in the sample B experimental series, whereas the PO_4^{3-} concentration decreases by max. ~86 % for sample A and M. In the latter case, the residual PO_4^{3-} load of the solution is increasing with increasing starting concentration (see. Fig. 3.2 for details).

In general, phosphate concentration decreases with increasing amount of calcite powder added to the solution. Depending on the starting phosphate concentration of the batch solution, total phosphate uptake by calcite increases more rapidly in sample B series in comparison to sample A and M (Fig. 3.2 & 3.3). These results show that the ability of phosphate uptake can be considered as a function of the SSA which is crucial in terms of adsorption and precipitation mechanisms and phase transformations, respectively.

To evaluate these mechanisms, sorption isotherms have been determined. These isotherms are in good agreement with those of *Eiche et al. (2008). Van Cappellen (1991)* divided sorption isotherms for phosphate on calcite into four sub-sections (Fig. 3.3 a) Section (A) marks a range of concentration of calcite (Cc) and PO_4^{3-} in which only adsorption on the calcite surface occurs (high Cc/PO_4^{3-} values). (B) shows the precipitation of meta-stable Ca-P compounds, (C) the transformation into stable

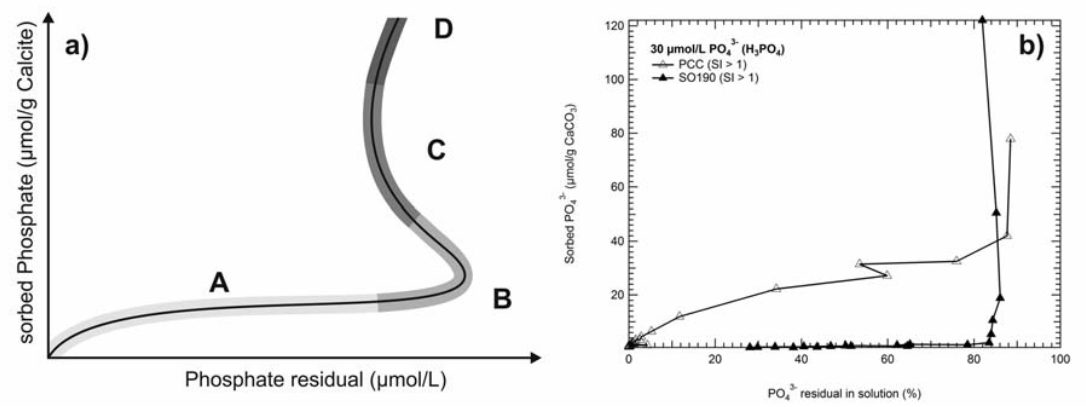

Figure 3.3: a) Schematic sorption isotherm for phosphate on calcite surfaces according to van Cappellen (1991), b) experimentally determined sorption isotherm for starting concentration of 30 µmol PO_4^{3-}/L.

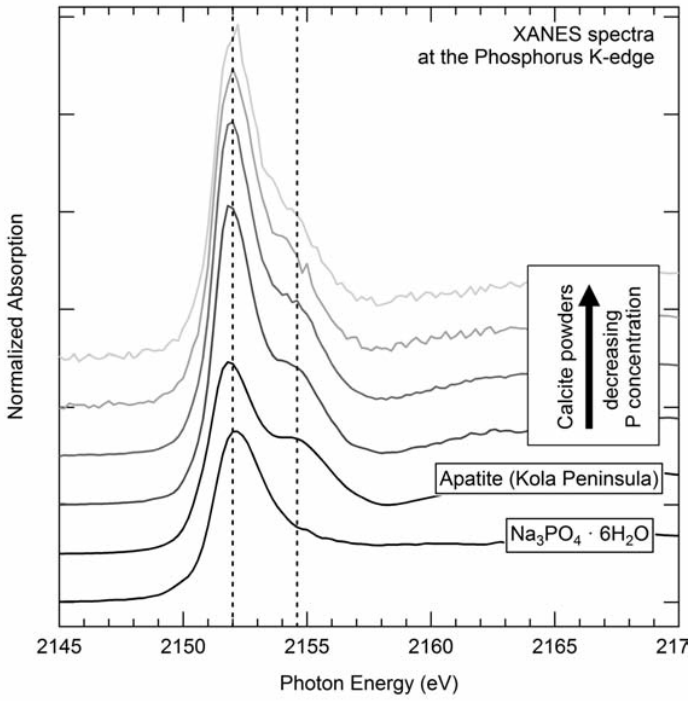

Figure 3.4: XANES spectra recorded at the P K-edge of phosphate-doped PCC powders and crystalline references materials, dashed lines mark energies at 2152.0 eV (phosphate »whiteline«) and 2154.6 eV. Analyses were conducted at the SUL-X and INE beamline at ANKA (KIT), respectively.

compounds and (D) the adsorption of phosphorus on the newly formed Ca-P surface (low Cc/PO_4^{3-}). These sections are different for the applied calcite powders of the experimental series. Figure 3.3 b) shows an example for experimentally determined sorption isotherms (30 µmol PO_4^{3-}/L) which can be divided in different sections. On the basis of these observations further analytical investigations will be carried out.

Processed calcite powders have been analysed using SEM imaging and, as a novel approach, XAFS spectroscopy (in particular XANES) is used to identify the speciation of phosphorus and phase transformations on the calcite surface. By applying these methods, a main goal is to understand the different phases of fixation and sorption and the transition zone (changeover from A to C in Fig. 3.3 a), respectively, on the calcite surface at the molecular scale.

First results show that XANES spectroscopy at the phosphorus K-edge is a suitable tool to identify the speciation of phosphorus on calcite (Fig. 3.4). Two characteristic features are observed at the P K-edge, the phosphate whi-

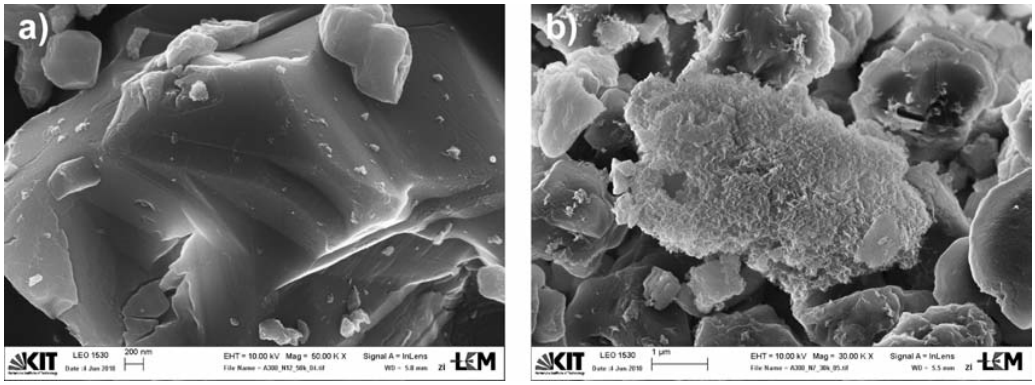

Figure 3.5: SEM images of processed limestone powders; a) section A, ~ 550 ppm P ≙ 6 at/nm2; b) section B, ~ 3600 ppm P ≙ 40 at/nm^2.

teline at 2152.0 eV and a shoulder at 2154.6 eV. The latter is characteristic for Ca-Phosphates and decreases with phosphorus concentration on the calcite powder, which shows a change in the coordination of phosphate. The analysed calcite samples are representative for parts (A) to (C) of the schematic sorption isotherm (see Fig. 3.3 a). SEM imaging has been perfomed for processed sample powders A and B. Only the limestone powder shows the occurrence of new phases in and therefore differences to the starting material. These phases have already been identified as Octa-Calcium-Phosphate (*Freeman and Rowell, 1981*).

3.3. Summary

Three calcite powders have been processed in batch sorption experiments. Based on the post-experimental solution chemistry, powders have been chosen for further analytical work. Merck $CaCO_3$, the limestone powder and the PCC powder show different shapes of the sorption isotherms. Phase transformations have been determined by SEM imaging for the limestone powder surfaces, but more detailed work including using SEM and EDX on all powders is necessary and in progress.

First XANES results at the P K-edge show two different spectral details and a change of the feature at 2154.6 eV with decreasing P concentration. Further XAFS spectroscopy (including XANES/EXAFS) at both the Ca K-edge (4038 eV) and the P K-edge (2146 eV) is planned. XPS and XRD analyses of the powders and AFM studies using Iceland spar single crystals, respectively, are in progress and will help to complete the characterisation of the atomic and molecular environment of phosphate at calcite surfaces.

4. Interactions of etidronic acid and PCC powders during the calcite crystal growth

Precipitated calcium carbonates (PCC), a purified, refined or synthetic calcium carbonate, are an industrial mass product commonly used during the production of pharmaceutical products, varnish and colours, paper, cosmetics and in the food processing industry (*e.g. Souto et al., 2008*). Moreover, organic additives such as etidronic acid (HEDP, HPO_3^{2+}), citric acid or tartaric acid are used in a wide field of industrial application of calcite chelating, dispersing or complexing agents in the production of paper, cosmetics and pharmaceutical products (*Dunn et al., 1994*). Our first experiments will focus on the interaction of HEDP during the calcite crystal growth.

First batch sorption experiments investigating the interaction of organic additives on the calcite crystal growth, especially of PCCs, were conducted in saturated and oversaturated calcite solutions and solution free of calcite. These solutions were produced as described in section 3.1. HEDP (etidronic acid, $C_2H_8O_7P_2$) was added in concentrations of 0 to 50 µmol/L (as organic agent) to the solution. For experiments 100 mg of calcite (Cc) powder (PCCs,

Merck p.a. $CaCO_3$, Iceland spar) varying in specific surface area (0.3 to 23.8 m^2/g) was added to 20 mL solution. Additionally, PCCs vary in crystal morphologies (scalenohedral, prismatic, rhombohedral). Afterwards, sample vials were closed and shaken for 24 h (Fig. 3.1). After the experiments, all solution were filtered and checked for alkalinity and pH. Ca^{2+} and P concentrations were determined AAS and/or ICP-OES. Phosphorus concentrations of the processed calcite powders were determined by EDXRF analyses.

pH values remained at 8.15 to 8.35 during the experimental run. (Over)saturated calcite solutions show decreasing trends for Ca^{2+} and HCO_3^- concentrations in dependence of the SSA. Differences can be observed in solutions where Cc powder with a max. SSA of ~2 m^2/g are used as crystal seeds. Here, the concentration of Ca^{2+} drops more efficiently when HEDP is available. Overall decrease of Ca^{2+} and HCO_3^- leads to a noticeable decrease of the calcite saturation, which was calculated using the PHREEQC software (*Parkhurst & Appelo, 1999*). Three experimental series with HEDP were conducted. Starting concentrations of 5 and 50 µmol/L were adjusted for (over)saturated calcite solutions and solutions without Ca^{2+} and HCO_3^- (Fig. 4.1). HEDP is eliminated from a pure etidronic acid solution by 80 to 90 %. Depending on the SSA of the applied Cc powder, up to 65 % of the starting HEDP is removed from the calcite solution. So far, no systematic interconnection of HEDP sorption and crystal morphology has been observed for SSA ~ 7 m^2/g. EDXRF analyses of Cc powders show P concentrations of 1000 to 1500 ppm.

First results show that the Ca^{2+} concentration of a calcite solution decreases stronger when HEDP is present. Differences in the decrease of HCO_3^- compared to solutions without HEDP have not been observed. From our experiments, this is valid for calcite powders with SSA ~ 2 m^2/g. This observation is supported by results reported by *Lin & Singer (2005)* or *Sawada et al. (2003)* and shows possible inhibition of calcite growth at these conditions due to precipitation Ca-P compounds. For HEDP a linear decrease dependent on the SSA of the Cc powder has been observed.

Changes in the calcite morphology and the P speciation and bonding at the calcite powder surfaces will be tracked using additional analytical methods (SEM, XRD, XPS, XAFS) and, furthermore, within in-situ AFM studies. Promi-

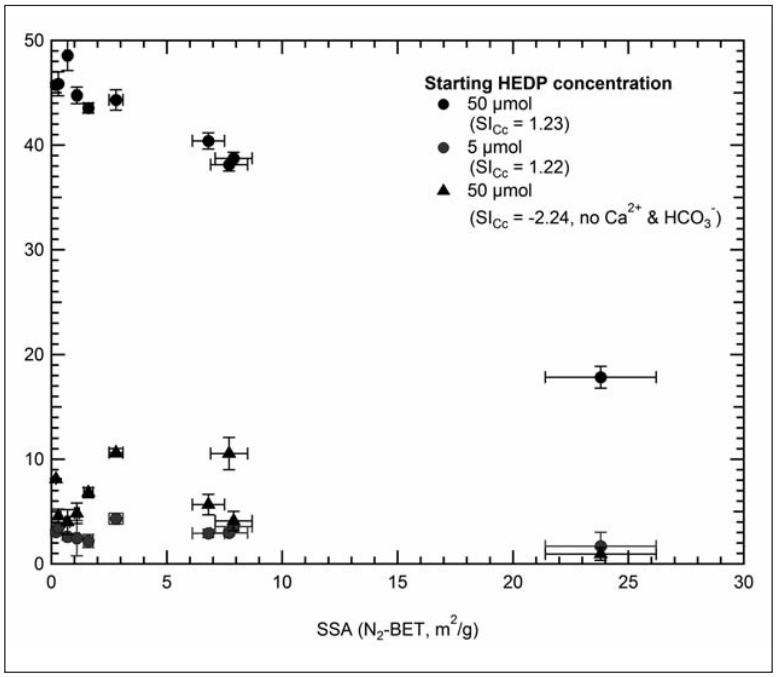

Figure 4.1: Remaining HEDP concentration in solution after experiment.

sing XANES measurements have been conducted at the P K-edge (Fig. 3.4), further analyses are planned.

5. Reactivity of calcite surfaces during concreting

Natural limestone plays a key role in the manufacturing of Portland cement and thus for the production of a broad bandwidth of building products, such as concrete. In order to reduce the ecological impact of modern cements, limestone is added to the cement as a filler material, thus reducing the cement clinker content. With increasing replacement rate, however, pronounced changes in the fresh and hardened concrete behaviour can be observed. At the fresh state, limestone strongly deteriorates the working mechanisms of modern concrete admixtures, such as superplasticizers, leading to pronounced problems in the placing and handling of the fresh concrete. This behaviour is normally attributed to the TOC content of the natural limestone, as this might interact with the organic matter of the superplasticizers. Systematic investigations regarding this important mechanism are not yet available. Further, limestone powder could be identified to trigger early hydration by acting as nucleus for the formation of calcium silicate hydrates, which are responsible for the strength of a hardened concrete (*Matschei et al., 2007*).

One of the primary goals of the research subproject described below, was to identify the interaction mechanisms of modern concrete superplasticizers with limestone powders (LSP) of different provenance and composition. On this basis, eluation tests investigating the dissolution behaviour of limestone in both an aqueous environment (carrier liquid water) and in an alkaline environment (pH 13, 1.0 mol/dm³ NaOH/KOH solution) were carried out. The volume fraction of solids in the solution was adjusted to be 5 vol.%, allowing for an undisturbed dissolution process far away from the saturation limit. Two types of superplasticizers, a polynaphtalene-sulphonate (PNS) which acts electrostatically and a polycarboxylate (PC) which acts sterically, were investigated. Each admixture was added to the carrier liquid at a dosage of 0.5 mass.% of the limestone. All investigations were carried out at 20 °C. The suspensions were continuously stirred during the investigation ensuring a homogeneous distribution of the particles in the carrier liquid. At certain time intervals, the pH value, conductivity and temperature of the solution were determined. Further, samples of 25 cm³ of the suspension were taken, filtrated and the filtrate was analyzed for its Ca, Mg and K ion content using the AAS method. Ca and Mg ions have been identified in earlier studies to have a significant influence on the rheological properties of the cement suspension (*Haist, 2009*).

As shown in Figure 5.1 (left), the Ca content in the carrier liquid strongly increases (background Ca content NaOH/KOH solution 0.14 g/dm³; NaOH/KOH + PC 0.41 g/dm³; NaOH/KOH+PNS 5.4 g/dm³) in the first minutes after addition of the solvent, indicating that pronounced quantities of limestone dissolve in the carrier liquid. This behaviour is independent of the presence of superplasticizer and the type of superplasticizer. After the first dissolution processes, the Ca content decreases again, indicating precipitation processes occurring in the solution. This process is identical for solutions with and without polynaphthalene-sulfonates. For suspensions containing the admixture on polycarboxylate basis, dissolution and precipitation processes seem to repeat several times, resulting in an oscillation of the total calcium content in the filtrate. The results further indicate, that the organic admixtures become chemically unstable over time and decompose after approx. 1400 min. (~24 h), resulting in a further decrease of the calcium content. Beyond this time, the precipitation process of calcium seems to continue, possibly accompanied by an oriented re-crystallization of calcium on the particle surface. However, from the logarithmic scaling of the time axis, no end-member could be identified from the measured data.

Plotting the calcium content in the filtrate eluated by the limestone normalized on calcium

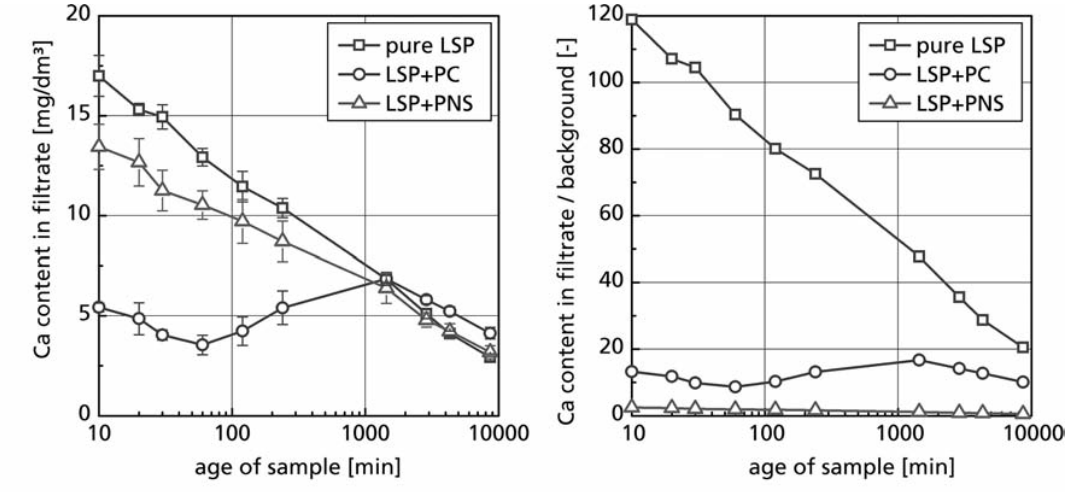

Figure 5.1: Calcium eluation of technical LSP in NaOH/KOH brine (pH 13, 1.0 mol/dm³) with and without superplasticizer based on polynaphthalin-sulfonate, PNS, or polycarboxylate, PC: absolute Ca content in filtrate (left) and content normalized by background (right).

content in the solution (with or without admixture), it becomes obvious, that the dissolution process of limestone and the release of calcium is strongly inhibited by the addition of both admixture types. The dissolution process itself is ascribed to the chemical instability of the limestone in the surrounding alkaline environment. Calcium dissolves from the surface of limestone powder and then precipitates again on the surface, possibly in a different crystal structure. At the same time there is an interaction of the superplasticizer with the calcite surface. This inhibits both the dissolution and the crystal growth, which could explain the time dependence of the calcium concentration in the normalized diagram (see Fig. 5.1, right). The eluation tests prove that limestone powder therefore interacts with both investigated superplasticizers, however in a different manor. In order to verify and characterise these processes in detail, surface sensitive analyses of the reactions between calcite and admixture will be carried out using AFM and ESEM methods. Additional eluation experiments are being carried out at the moment.

Based on the results of the eluation tests, combined rheological and electro-acoustical investigations on pure limestone powder suspensions and cement suspension with limestone powder fractions were carried out. The rheological behaviour of the suspension was determined using both oscillatory and rotational rheometer tests. First results of the rheological tests have been reported in (*Müller et al., 2009*). At the same time, the zeta potential of the particles and the medium agglomerate size in the suspension are determined in situ using electro-acoustical measurement techniques. Therefore, a defined AC voltage is applied to the sample, resulting in an electrical field in the suspension. In case the suspended particles are electrically charged with a charge of ζ (zeta potential in mV), the particles start to oscillate in the electrical field of amplitude E resulting in an oscillating pressure wave in the incompressible carrier liquid. This pressure signal is recorded using an ultrasound transducer. From the amplitude of the pressure signal p, the zeta potential ζ can be calculated using Eq. 5.1:

$$\zeta = \frac{p}{E} \cdot \frac{1}{(\rho_p - \rho_s) \cdot c \cdot \phi} \cdot \frac{3\eta_s}{2\varepsilon_0 \varepsilon_r} \cdot \frac{1}{G(\alpha) \cdot (1 + f(\lambda, \omega'))}$$

In Eq. 5.1 ρ_p and ρ_s denote the density of the particle and the carrier liquid, respectively. The parameter c denotes the speed of sound in the carrier liquid. The phase content ϕ in the tests was set to 0.44. η_s, ε_0 and ε_r describe the dynamic viscosity, the specific dielectrical constant and the permittivity of the carrier liquid. $G(\alpha)$ and $f(\lambda,\omega')$ are correction terms. For further details regarding this measurement technique see (*Haist et al., 2009*).

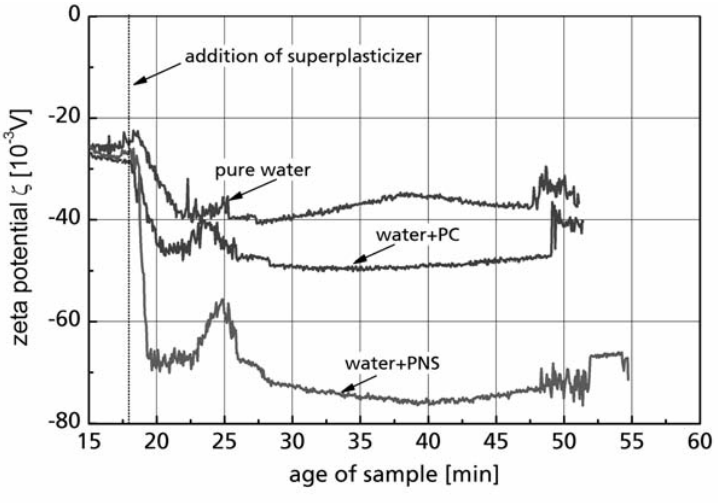

Figure 5.2: Temporal development of the zeta potential of limestone powder (LSP) in pure water, water and polycarboxylate (PC) and water and polynaphthalin-sulfonate (PNS).

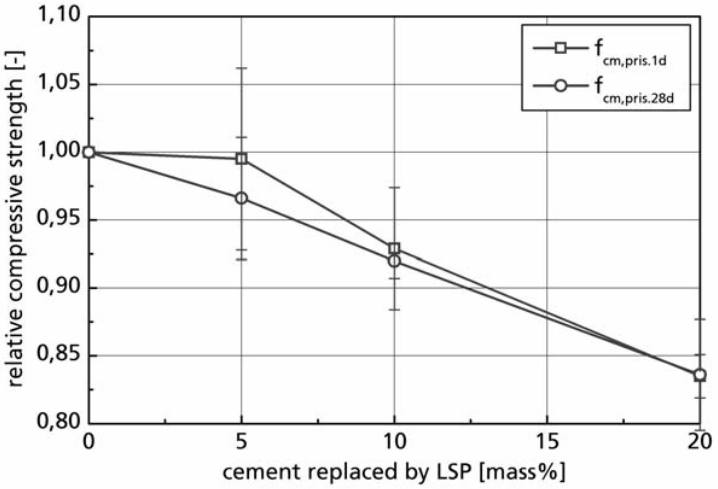

Figure 5.3: Influence of the cement replacement by limestone powder (LSP) on the compressive strength determined on prismatic specimens (40x40x160 mm³) normalized by the compressive strength of specimens with pure cement.

Figure 5.2 shows the influence of different types of superplasticizers on the zeta potential of limestone powder particles suspended in water. Both the addition of polycarboxylate (PC) as well as the addition of polynaphthalin-sulfonate (PNS) leads to a strong reduction of the zeta potential of the particles. For the admixture on PNS basis, this reduction is more pronounced than for the one on PC basis. However, also the suspension without superplasticizer addition shows significant changes in the zeta potential in a time frame between 17 and 25 min. after addition of water to the dry powder. The reasons for this reduction are assumed to be linked to the calcium eluation and re-precipitation observed in the eluation tests. However, the mechanisms for this process still have to be clarified by additional tests. The same is true for the pronounced peak in the zeta potential time curve at the age of approx. 23 to 25 min. This peak is observed independent of the presence and the type of superplasticizer and also has to be clarified.

The long-term influence of the cement replacement by limestone powder was studied using tests on hardened concrete. Therefore, prismatic specimens measuring 40 x 40 x 160 mm³ were casted from the different cement pastes, demolded after one day and stored in water until testing. On the specimens, the compressive and the bending tensile strength were determined according to DIN EN 196-1.

As shown in Figure 5.3, the replacement of cement by limestone powder leads to a systematic decrease in the compressive strength. The reduction of cement, however, is not identical to the reduction in strength. Despite the large scat-

ter, for cement replacements by LSP of up to 20 mass.%, a cement reduction by 1 % leads to a reduction of compressive strength of approximately 0.7 % for the investigated limestone powder. Further investigations are in progress.

6. Thermodynamics of mixing in carbonate solid solutions from atomistic simulations

In the past project period we have successfully modelled the thermodynamics of cationic, $(Ca/Mg)^{2+} = Cd^{2+}$ and anionic, $(CO_3)^{2-} = (SO_4/SeO_4)^{2-}$ substitutions in carbonates. The solid solutions have been modelled with two different atomistic simulation approaches, namely, the Double Defect Method (DDM) (*Vinograd et al., 2009*) and the Single Defect Method (SDM), which we have developed for iso-structural and non-iso-structural substitutions, respectively. The substitution $(Ca/Mg)^{2+}=Cd^{2+}$ has been studied within two binary sections of the ternary system $CaCO_3$-$MgCO_3$-$CdCO_3$. The description of the binary section $(Ca_{0.5}Mg_{0.5})CO_3$-$(Cd_{0.5}Mg_{0.5})CO_3$, dolomite-Cd-dolomite, required the development of a ternary version of the DDM (*Vinograd et al., 2010*), which was accomplished within the project. The modelling of the non-iso-structural solid solutions $CaCO_3$-$CaSO_4$ and $CaCO_3$-$CaSeO_4$ with calcite and aragonite structure types was performed using the SDM. The SDM provides an algorithm for the calculation of the thermodynamic properties of virtual end-members with the compositions of $CaSO_4$ and $CaSeO_4$, which involves simulation of supercell structures of the host phases ($CaCO_3$ calcite/aragonite) with one CO_3^{2-} unit replaced with a SO_4^{2-} or SeO_4^{2-} unit.

6.1. The system $CaCO_3$-$MgCO_3$-$CdCO_3$

The main aim of this study was to derive the mixing properties along the $CaCO_3$-$CdCO_3$ (calcite) and $(Ca_{0.5}Mg_{0.5})CO_3$-$(Cd_{0.5}Mg_{0.5})CO_3$ (dolomite) binaries and thus to be able to model the co-precipitation of Cd^{2+} with calcite and dolomite. The secondary aim was to provide an additional test for a new set of empirical pair potentials for Ca,Mg-carbonates developed by *Raiteri et al. (2010)*. The new force-field model has shown excellent performance in the description of relative stability of all known polymorphs of $CaCO_3$ and of hydration properties of calcite. The task was to test its accuracy in predicting the effects of mixing in the solid solutions. These aims essentially required us to model the mixing properties within the ternary system. The binary systems were modelled with the standard DDM (*Vinograd et al., 2009*). The simulation results are in the excellent agreement with the available experimental data. The mixing in the calcite-otavite binary is essentially ideal. This is in an agreement with the recent experimental data of *Katsikopoulos et al. (2008)*. The calcite-dolomite and otavite-dolomite binaries show the tendency to the formation of the ordered intermediate compounds with the dolomite structure. The predicted subsolidus phase relations are in good agreement with the experimental data of *Goldsmith and Heard (1961)* and *Goldsmith (1972)*. The temperature-composition diagrams are shown in Figure 6.1 a) & b). Here we wish to emphasize that this agreement did not required any adjustment of the force-field parameters of *Raiteri et al. (2010)*. The Cd-O potential was obtained by fitting to the formation energies of several ordered compounds in the otavite-magnesite system calculated quantum-mechanically by *Burton and van de Walle (2003)*. The obtained agreement with the experimental data within the binaries suggests that the model is sufficiently accurate for the compositions within the ternary system. Figure 6.2 shows the free energy of mixing in the ternary system at 873 K calculated with the ternary DDM. The miscibility gaps are shown in the projection of the free energy surface onto the ground plane. In Figure 6.3 the activities of the solid solutions with the calcite and dolomite structures are compared. Our results suggest that the mixing of Cd and Ca within the ordered dolomite structure is less ideal than within the calcite-otavite binary. This is the effect of the third component, $MgCO_3$. The increase in »non-ideality« is due the contraction of the dolomite lattice relative to the structure of calcite, which is caused by the presence of compact Mg-layers. The next step of our research will be

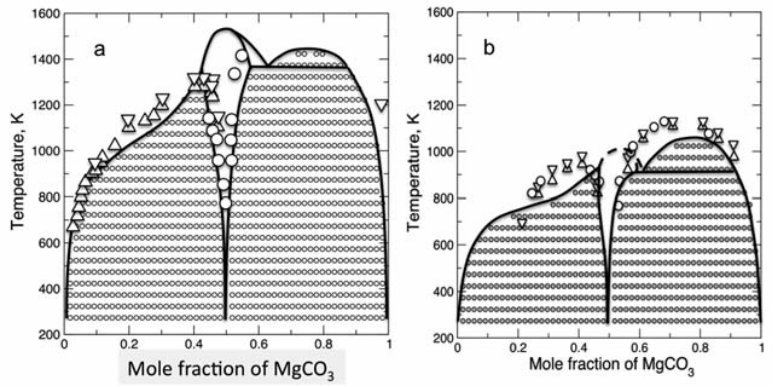

Figure 6.1: The subsolidus phase relations in calcite-magnesite (a) and otavite-magnesite (b) systems simulated with the Monte Carlo method using the pairwise interactions computed with the DDM. The symbols are the experimental data from *Goldsmith and Heard (1961)* (a) and *Goldsmith (1972)* (b), respectively.

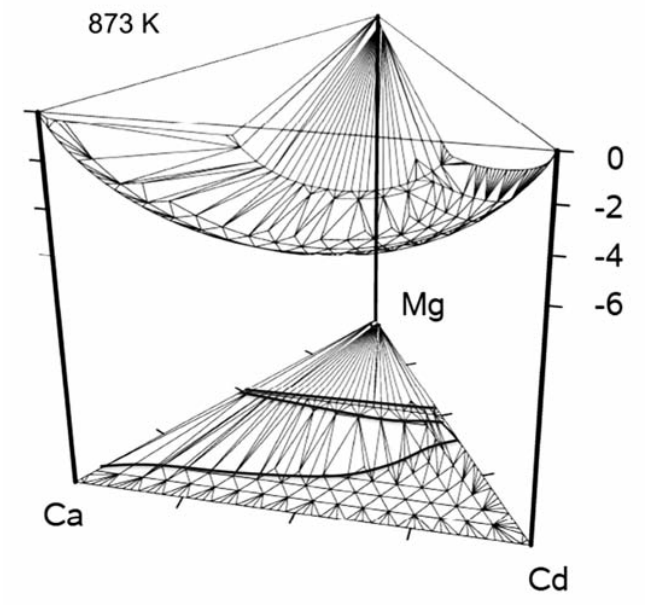

Figure 6.2: The Gibbs free energy of mixing in the calcite-magnesite-otavite, $CaCO_3$-$MgCO_3$-$CdCO_3$, system at 873 K simulated with the Monte Carlo method using the pairwise interactions computed with the ternary DDM. The solid curves outline the boundaries of the miscibility gaps.

to use the predicted activity-composition relations for the calculation of Lippmann diagrams and for the assessment of relative retention capacity of calcite and dolomite for Cd^{2+}.

6.2. The solid solutions of $CaCO_3$-$CaSO_4$ and $CaCO_3$-$CaSeO_4$ in calcite and aragonite

The thermodynamic description of these solid solutions is problematic. Indeed, all available solid solution theories including the DDM consider iso-structural solid solutions. The theory requires that the both end-members should belong to the same space group. This condition cannot be fulfilled, as it is not possible to build two iso-structural end-members due to the different geometry of CO_3^{2-} and SO_4^{2-}/SeO_4^{2-} groups. The fortunate circumstance is that due to the structural difference, these solid solutions are very dilute. Diluted solid solutions are typically very disordered and thus, the regular model description is adequate. Figure 6.4 shows the enthalpies of mixing of two hypothetical regular solid solutions with calcite and anhydrite structure types, for which complete sets of the end-members are unavailable. We are concerned with the description of mixing in the vicinity of pure calcite only. The enthalpy of mixing of a regular solid solution in the diluted range can be well modelled with a linear equation, which forms a tangent to the enthalpy of mixing curve. The white circle denotes the excess enthalpy of a supercell structure of calcite with a single defect of SO_4^{2-} substituting for CO_3^{2-}. The enthalpy of this

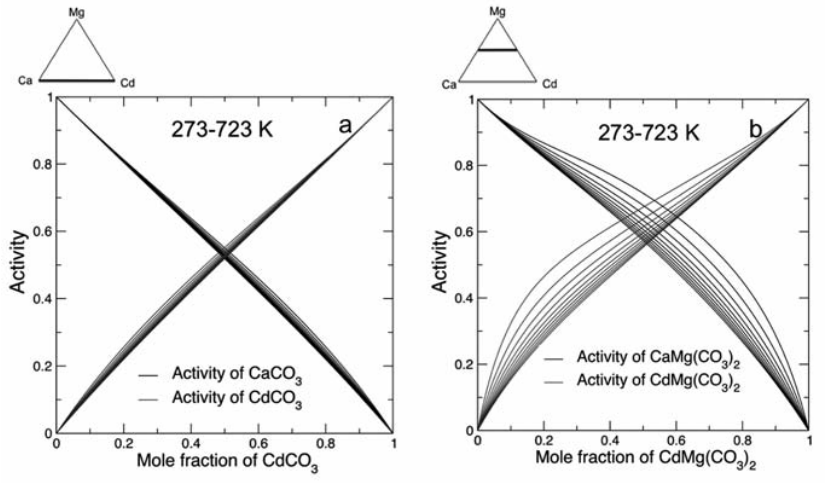

Figure 6.3: The activity-composition relations in calcite-otavite (a) and dolomite-Cd-dolomite (b) solid solutions computed with the Monte Carlo method.

Table 6.1: The total energies of the supercell structures and the total energies of the virtual end-members in eV calculated with SDM. The last column shows the energy of reference compounds, whose thermo- dynamic properties are assumed to be known.

Host phase	Single defect structure	Virtual end-member	Reference compound
$Ca_{16}(CO_3)_{16}$	$Ca_{16}(CO_3)_{15}SO_4$	$CaSO_4$ (in calcite)	$CaSO_4$ (anhydrite)
-39448.321	-40005.622	-3022.821	-3023.859
$Ca_{16}(CO_3)_{16}$	$Ca_{16}(CO_3)_{15}SO_4$	$CaSO_4$ (in aragonite)	$CaSO_4$ (anhydrite)
-39447.490	-40003.622	-3021.921	-3023.859
$Ca_{16}(CO_3)_{16}$	$Ca_{16}(CO_3)_{15}SeO_4$	$CaSeO_4$ (in calcite)	$CaSeO_4$ (anhydrite)
-39448.321	-39983.964	-3001.163	-3002.456
$Ca_{16}(CO_3)_{16}$	$Ca_{16}(CO_3)_{15}SeO_4$	$CaSeO_4$ (in aragonite)	$CaSeO_4$ (anhydrite)
-39447.490	-39982.142	-3000.120	-3002.466

The calculations are performed with CASTEP in DFT GGA approximation with PBESOL functional at 0 GPa

structure necessarily belongs to the enthalpy of mixing function of the disordered solid solution, because a structure with a single defect cannot have any ordering. The enthalpy of this structure also falls on the tangent, because the ratio of solute to host concentration is small. This implies that if it was possible to define a virtual end-member, which enthalpy falls on the tangent line, then such a solid solution would be strictly ideal. The single defect method is based on the notion that the enthalpy of the virtual end-member can be calculated knowing the absolute enthalpy of the single defect structure, the enthalpy of the host phase and the number of the exchangeable units in the supercell. Figure 6.5 shows the supercell structures of calcite and aragonite with a single defect of SO_4^{2-} used in the study. Table 6.1 shows the results of the calculation of the enthalpies of virtual compounds with $CaSO_4$ and $CaSeO_4$ composition, which form ideal solid solutions with calcite and aragonite. The standard enthalpies of the virtual compounds can be calculated knowing the standard enthalpy of a stable compound, which has the same composition as the virtual compound. Clearly, the enthalpy of this compound should be calculated with the same atomistic simulation approach, which was used to calculate the properties of the virtual end-member. In the case of the $CaCO_3$-$CaSO_4$ solid solution $CaSO_4$ anhydrite is a natural choice for the reference compound. In the case of the $CaCO_3$-$CaSeO_4$ system, a stable compound with $CaSeO_4$ composition does not exist. However, there is a possibility to estimate the standard properties of a compound iso-structural to anhydrite from the reaction (Eq.6.1.)

$$CaSeO_4 + CaSO_4 \times 2H_2O = CaSO_4 + CaSeO_4 \times 2H_2O$$

where $CaSeO_4 * 2H_2O$ is a well characterized compound iso-structural to gypsum. Our quantum-mechanical calculations suggest that the enthalpy change due to the reaction in Eq.

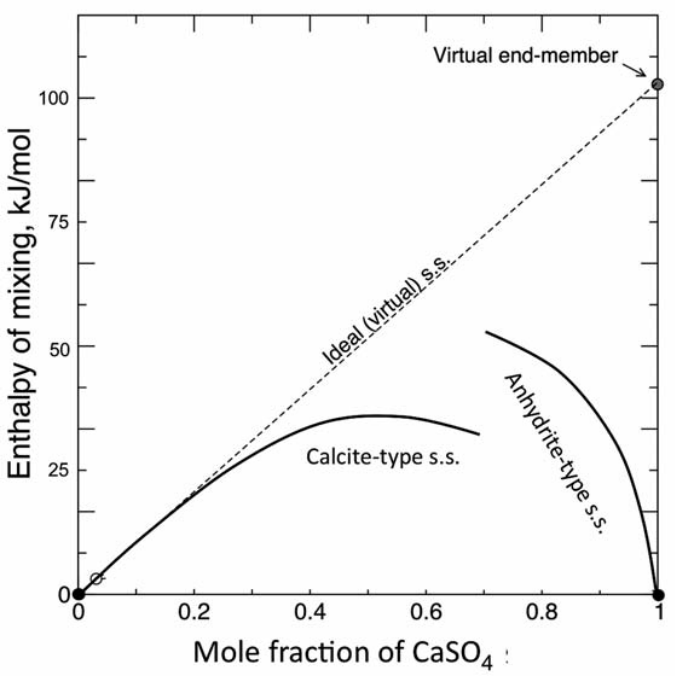

Figure 6.4: The virtual end-member construction for $CaCO_3$-$CaSO_4$ system. The solid circles are the stable host phases with calcite and anhydrite structures. The white circle is the excess energy of a supercell of calcite with one CO_3^{2-} group replaced with a SO_4^{2-} group. The grey circle is the enthalpy of the virtual $CaSO_4$ end-member, which corresponds to ideal calcite-type solid solution.

6.1 is -10.85 kJ/mole. Neglecting the entropy change in this reaction and using thermodynamic data for $CaSeO_4$*$2H_2O$, $CaSO_4$(anhydrite) and $CaSO_4$*$2H_2O$ (gypsum) from the Nagra-PSI data base (*Hummel et al., 2002*), we obtained -996.87 kJ/mol for the standard Gibbs free energy of $CaSeO_4$ (anhydrite). Our next concern was to estimate the standard entropies of the virtual end-members $CaSO_4$ (in calcite) and $CaSO_4$ (in aragonite) by calculating the phonon density of states of the relevant supercell structures. The lattice dynamics calculations were performed with the program GULP (*Gale and Rohl, 2003*). The force-field model was combined from the model of *Allan et al. (1993)* for sulphates and a new model of *Raiteri et al. (2010)* for carbonates. These calculations have shown that the standard entropies of the virtual compounds $CaSO_4$ (in calcite) and $CaSO_4$ (in aragonite) are 121.7 and 142.8 J/mol/K, respectively. Knowing the standard entropy of $CaSO_4$ (anhydrite) of 105.32 J/mol/K, and using the enthalpy values from Table 6.1, we obtained the values of -1226.41 and -1145.87 for the standard Gibbs free energies of $CaSO_4$ (in calcite) and $CaSO_4$ (in aragonite), respectively. Assuming that the entropy changes of the reactions

$$CaSeO_4 \text{ (in calcite)} = CaSeO_4 \text{ (anhydrite)}$$

(Eq. 6.2)

and

$$CaSeO_4 \text{ (in aragonite)} = CaSeO_4 \text{ (anhydrite)}$$

(Eq. 6.3)

are the same as in the analogous reactions for sulphates, we obtained the values of -877.11 and -781.81 kJ/mol for the standard Gibbs free energies of $CaSeO_4$ (in calcite) and $CaSeO_4$ (in aragonite), respectively.

The obtained values permit straightforward calculations of the retention levels of SO_4^{2-} and SeO_4^{2-} in carbonates equilibrated with aqueous solutions. Assuming that the maximum possible ion activity product $[Ca^{2+}][SO_4^{2-}]$ in aqueous solutions is limited by the equilibrium solubility product of $CaSO_4$*$2H_2O$ (gypsum), we can calculate the maximum retention levels of SO_4^{2-} in calcite and aragonite from the reactions:

$$CaSO_4 \text{ (in calcite)} = CaSO_4 \times 2H_2O \text{ (gypsum)} - 2H_2O$$

(Eq. 6.4)

$$CaSO_4 \text{ (in aragonite)} = CaSO_4 \times 2H_2O \text{ (gypsum)} - 2H_2O$$

(Eq. 6.5)

The maximum retention levels of SeO_4^{2-} can be obtained from the analogous reactions:

$$CaSeO_4 \text{ (in calcite)} = CaSeO_4 \times 2H_2O - 2H_2O$$

(Eq. 6.6)

$$CaSeO_4 \text{ (in aragonite)} = CaSeO_4 \times 2H_2O - 2H_2O$$

(Eq. 6.7)

The equilibrium concentration of SO_4^{2+} in calcite according to Eq. 6.4 is defined by the equation

$$RT \cdot \ln x\left(SO_4^{2-}\right) = \Delta G_f^0\left(CaSO_4 \cdot 2H_2O\right) - 2 \cdot \Delta G_f^0\left(CaSO_4(calcite)\right)$$
$$= -1797.24 + 474.26 + 1226.41 = -96.57 kJ/mol$$

(Eq. 6.8)

Therefore, the maximum equilibrium retention level of SO_4^{2-} in calcite at 298 K is $1.3*10^{-17}$. The analogous calculations for aragonite give an even smaller value of $8.3*10^{-32}$. The retention levels of SeO_4^{2-} in calcite and aragonite calculated using the reactions in Eq. 6.6 and Eq. 6.7 are $7.4*10^{-24}$ and $1.5*10^{-40}$, respectively. These small values are essentially determined by the predicted large enthalpies of the virtual compounds relative to the enthalpies of the anhydrite-type phases.

6.3. Summary

Our results show that quantum-mechanical calculations and force-field modelling provide useful tools for predicting equilibrium retention levels of hazardous components in carbonate minerals. Particularly, we have demonstrated that the DDM is able to quantitatively predict mixing properties of various iso-structural binary and ternary carbonate solid solutions. We have also demonstrated the possibility of a quantitative modelling of non-iso-structural solid solutions with the SDM.

The particularly interesting result is that the equilibrium retention levels of SO_4^{2-} and SeO_4^{2-} in carbonates are very low. This implies that the reasonably large concentrations SO_4^{2-} and SeO_4^{2-} in carbonates reported in literature (*Reeder et al., 1994; Pingitore et al., 1995*) should be attributed to non-equilibrium entrapment effects.

7. Conclusion and Outlook

In the past project period, promising and useful results with regard to industrial application have been achieved. The calcite(104)-water interface has been characterised by in-situ surface diffraction under varying hydrochemical conditions. Moreover, experimental results investigating the interaction of the calcite sur-

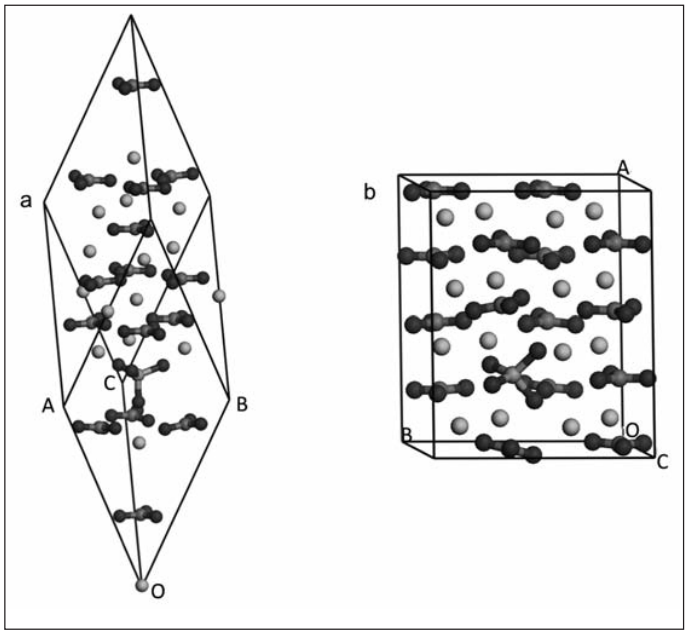

Figure 6.5: The relaxed 2x2x2 and 2x2x1 supercells of calcite (a) and aragonite (b) with one CO_3^{2-} unit replaced with SeO_4^{2-} unit. The geometry minimization calculations were performed with CASTEP in GGA-PBE approximation.

face and Se show that calcite is an efficient medium to immobilise oxianions and EXAFS studies characterized the adsorption species of Se, respectively.
Elimination of phosphate from calcite solutions by calcite powders shows that P fixation is predominantly a function of the specific surface area. Occurrence of sorption mechanisms, new Ca-P phases and phase transitions, respectively, is different for each applied calcite powder. Systematic SEM and EDX studies accompanied by further XRD and XAFS analyses will indicate points of changeover from sorption to precipitation. Additional AFM studies will help to understand inhibition and/or growth mechanisms on the calcite powder and single crystal surfaces. The results achieved to date provide a basis for forthcoming experimental and analytical work and are promising for advances in the application of calcite materials in water treatment and phosphate recycling, respectively.
Experiments investigating the interactions of limestone powder and superplasticizers, with regard to concreting, show uncommon dissolution and re-crystallisation pattern of calcite at alkaline conditions. Further analytical work is necessary to describe the observed behaviour of the admixtures during the experimental run-time.
Results of quantum-mechanical calculations and force-field modelling are useful to predict equilibrium retention levels calcite minerals. In the following project period, these methods will try to solve or support specific problems investigated with experimental methods in the lab.

Acknowledgements
We wish to thank Dr. Dmitrii Kulik, Dr. Enzo Curti (Paul Sherrer Institute, Switzerland), Prof. Julian D. Gale (Curtin University, Perth, Australia) for the help in this project. The atomistic calculations were performed at the Center for Scientific Computing at the University of Frankfurt.

The ANKA (KIT) beamline staff at SUL-X (Jörg Göttlicher, Ralph Steininger) and INE (Jörg Rothe, Kathy Dardenne) is greatly acknowledged for support during test analyses and beamtime measurements. Hartmut Gliemann is acknowledged for support during AFM analyses at the Institute of Functional Interfaces (KIT-IFG).

References

Austen, K., Wright, K., Slater, B. & Gale J.D. (2005) The interaction of dolomite surfaces with metal impurities: a computer simulation study. Phys. Chem. Chem. Phys. 7, 4150–4156.

Babin, J., Prepas, E.E., Murphy, T.P., Serediak, M., Curtis, P.J., Zhang, Y. & Chambers, P.A. (1994) Impact of lime on sediment phosphorus release in hardwater lakes: The case of hypereutrophic Halfmoon Lake, Alberta. Lake and Reservoir Management 8, 131-142.

Belzile, N., Pizarro, J., Filella, M. & Buffle, J. (1996) Sediment diffusive fluxes of Fe, Mn, and P in a eutrophic lake: Contribution from lateral vs. bottom sediments. Aquatic Sciences - Research Across Boundaries 58, 327-354.

Berg, U., Neumann, T., Donnert, D., Nüesch, R. & Stüben, D. (2004) Sediment capping in eutrophic lakes - efficiency of undisturbed calcite barriers to immobilize phosphorus. Appl. Geochem. 19, 1759-1771.

van Cappellen, P. (1991) The formation of marine apatit - A kinetic study. PhD thesis, Yale University, New Haven.

van Cappellen, P., Charlet, L., Stumm, W. & Wersin, P. (1993) A surface complexation model of the carbonate mineral-aqueous solution interface. Geochim. Cosmochim. Acta 57, 3505-3518.

Casey, W.H., Rock, P.A., Chung, J-B., Walling, E.M. & McBeath, M.K. (1996) Gibbs energies of formation of metal-carbonate solid solutions 2: the CaxSr1-xCO3 system at 298 K and 1 bar. Am. J. Sci. 296, 1–22.

Clark, S. J., Segall, M. D., Pickard, C. J., Hasnip, P. J., Probert, M. J., Refson, K. & Payne, M. C. (2005) First principles methods using CASTEP. Zeitschrift fuer Kristallographie 220, 567-570.
Driver, J., Lijmbach, D. & Steen, I. (1999) Why Recover Phosphorus for Recycling, and How?. Environ. Technol. 20, 651-662.

Dunn, C.J., Fitton, A. & Sorkin, E.M. (1994) Etidronic Acid - A Review of Its Pharmacological Properties and Therapeutic Efficacy In Resorptive Bone-disease. Drugs & Aging 5, 446-474.

Eiche, E.; Berg, U.; Song, Y. & Neumann, T. (2008) Fixation and Phase Transformation of Phosphate at Calcite Surfaces – Implications for Eutrophic Lake Restoration Australasian Institute of Mining and Metallurgy Bulletin, 292-302.

Freeman, J. S. & Rowell, D. L. (1981) The adsorption and precipitation of phosphate onto calcite. Europ. J. Soil Sci. 32, 75-84.

Gale, J.D. & Rohl, A.L. (2003) The General Utility Lattice Program (GULP). Molecular Simulations 29, 291-341.

Gilbert, N. (2009) Environment: The disappearing nutrient. Nature 461, 716-718.

Goldsmith, J.R. & Heard, H.C. (1961) Subsolidus phase relations in the system CaCO3-MgCO3. J. Geology 69, 45-74.

Goldsmith, J.R. (1972) Cadmium dolomite and the system CdCO3-MgCO3. J. Geology 80, 617-626.

Hummel, W., Berner, U.R., Curti, E., Pearson, F.J. & Thoenen, T. (2002) Nagra/PSI chemical thermodynamic data base 01/01. Radiochim. Acta 90, 805-813.

Haist, M. (2009) Zur Rheologie und den physikalischen Wechselwirkungen bei Zementsuspensionen. Dissertation Universität Karlsruhe (TH), Germany.

Hart, B., Roberts, S., James, R., Taylor, J., Donnert, D. & Furrer, R. (2003) Use of active barriers to reduce eutrophication problems in urban lakes. Water Sci. Technol. 47, 157-163.

Katsikopoulos, D., Fernandez-Gonzalez, Á. & Prieto, M. (2008) Crystallization of the (Cd,Ca) CO_3 solid solution in double diffusion systems: the partitioning behaviour of Cd^{2+} in calcite at different supersaturation rates. Min. Mag. 72, 433-436.

Kulik, D.A., Berner, U. & Curti, E. (2004) Modelling chemical equilibrium partitioning with the gems-psi code. In B. Smith and B. Gschwend, editors, PSI Scientific Report 2003. Nuclear Energy and Safety IV, Villigen. Paul Scherrer Institut.

Kulik, D.A., Vinograd, V.L., Paulsen, N. & Winkler, B. (2010) $(Ca,Sr)CO_3$ aqueous-solid solution systems: From atomistic simulations to thermodynamic modelling. Phys. Chem. Earth 35, 217-232.

Lin, Y.-P. & Singer, P. C. (2005) Inhibition of calcite crystal growth by polyphosphates. Water Res. 39, 4835-4843.

Matschei, Th., Lothenbach, B., Glasser, F. P. (2007) The role of calcium carbonate in cement hydration. In: Cement and Concrete Research 37, 551-558.

Müller, H. S., Haist, M., Glowacky, J. (2009) Reactivity of calcite surfaces during concreting. In: GEOTECHNOLOGIEN Statusbericht 2009, Universität Bayreuth, November 2009.

Parkhurst, D.L. & Appelo, C.A.J. (1999) User's Guide To PhreeqC (version 2) - A Computer Program For Speciation, Batch-reaction, One-dimensional Transport, And Inverse Geochemical Calculations. U.S. Geological Survey.

Perdew, J.P., Burke, K. & Ernzerhof, M. (1996) Generalized gradient approximation made simple. Phys. Rev. Lett. 77, 3865-3868.

Pingitore, N.E., Meitzner, G. & Love, K.M. (1995) Identification of sulfate in natural carbonates by X-ray absorption spectroscopy. Geochim. Cosmochim. Acta 59, 2477-2483.

Pokrovsky, O. S., Mielczarski, J. A., Barres, O. & Schott, J. (2000) Surface speciation models of calcite and dolomite/aqueous solution interfaces and their spectroscopic evaluation. Langmuir 16, 2677-2688.

Prepas, E.E., Murphy, T.P., Dinsmore, W.P., Burke, J.M., Chambers, P.A. & Reedyk, S. (1997) Lake Management Based on Lime Application and Hypolimnetic Oxygenation: the Experience in Eutrophic Hardwater Lakes in Alberta. Water Qual. Res. J. Can. 32, 273-293.

Raiteri, P., Gale, J.D., Vinograd, V.L. & Winkler, B. (2010) A computational investigation of the bulk and aqueous surface properties of calcite, magnesite and dolomite (in preparation)

Reeder, R.J., Lamble, G.M., Lee, J-F. & Staudt, W.F. (1994) Mechanism of SeO42-substitution in calcite: An XAFS study. Geochim. Cosmochim. Acta 58, 5639-5646.

Sawada, K., Abdel-Aal, N., Sekino, H. & Satoh, K. (2003) Adsorption of inorganic phosphates and organic polyphosphonate on calcite. Journal of the Chemical Society. Dalton Transactions, 342-347.

Smith, V.H. (2003) Eutrophication of freshwater and coastal marine ecosystems - A global problem. Environ. Sci. Poll. Res. 10, 126-139.
Somasundaran, P. & Agar, G.E. (1967) Zero Point of Charge of Calcite. J. Colloid Interface Sci. 24, 433-440.

Souto, E.C.S., Damasceno, J.J.R. & Hori, C.E. (2008) Study of Operational Conditions for the Precipitated Calcium Carbonate Production. Advanced Powder Technology VI 591-593, 526-530.

Vinograd, V.L., Sluiter, M.H.F. & Winkler, B. (2009) Subsolidus phase relations in the $CaCO_3$-$MgCO_3$ system predicted from the excess enthalpies of supercell structures with single and double defects. Phys. Rev. B 79,10420-104209.

Vinograd, V.L., Paulsen, N., Winkler, B. & van de Walle, A. (2010) Thermodynamics of mixing in the ternary rhombohedral carbonate solid solution $(CaxMgyMn1–x–y)CO_3$ from atomistic simulations. CALPHAD 34,113-119.

Wolthers, M., Charlet, L. & van Cappellen, P. (2008) The Surface Chemistry of Divalent Metal Carbonate Minerals; a critical Assessment of Surface Charge and Potential Data using the Charge Distribution Multi-Site Ion Complexation Model. Am. J. Sci. 308, 905-941.